Superpixel-Based Fast Fuzzy C-Means Clustering for Color Image Segmentation

Tao Lei , *Member, IEEE*, Xiaohong Jia, Yanning Zhang, *Senior Member, IEEE*, Shigang Liu, Hongying Meng , *Senior Member, IEEE*, and Asoke K. Nandi , *Fellow, IEEE*

Abstract—A great number of improved fuzzy c-means (FCM) clustering algorithms have been widely used for grayscale and color image segmentation. However, most of them are time-consuming and unable to provide desired segmentation results for color images due to two reasons. The first one is that the incorporation of local spatial information often causes a high computational complexity due to the repeated distance computation between clustering centers and pixels within a local neighboring window. The other one is that a regular neighboring window usually breaks up the real local spatial structure of images and thus leads to a poor segmentation. In this work, we propose a superpixel-based fast FCM clustering algorithm that is significantly faster and more robust than state-of-the-art clustering algorithms for color image segmentation. To obtain better local spatial neighborhoods, we first define a multi-scale morphological gradient reconstruction operation to obtain a superpixel image with accurate contour. In contrast to traditional neighboring window of fixed size and shape, the superpixel image provides better adaptive and irregular local spatial neighborhoods that are helpful for improving color image segmentation. Second, based on the obtained superpixel image, the original color image is simplified efficiently and its histogram is computed easily by counting the number of pixels in each region of the superpixel image. Finally, we implement FCM with histogram parameter on the superpixel image to obtain the final segmentation result. Experiments performed on synthetic images and real images demonstrate that the proposed algorithm provides better segmentation results and takes less time than state-of-the-art clustering algorithms for color image segmentation.

Index Terms—Color image segmentation, fuzzy c-means (FCM) clustering, morphological reconstruction, superpixel.

I. INTRODUCTION

IMAGE segmentation is a key step of object recognition and classification in computer vision. Although a large number of algorithms used for image segmentation have been proposed, image segmentation remains one of the most challenging research topics because none of them is able to provide a unified framework for achieving fast and effective image segmentation. The difficulty of image segmentation can be attributed to two reasons. The first is that image segmentation is a multiple solution problem, i.e., there are multiple best segmentation results for one image. The second is that an image is always complex because of noise, background, low signal-to-noise ratio, and intensity nonuniformity. Consequently, it is difficult to propose a general segmentation framework to achieve complex image segmentation tasks.

Image segmentation algorithms can be roughly grouped into two categories—unsupervised and supervised image segmentation. Unsupervised approaches, such as clustering [1], [2], GraphCut [3], active contour model [4], watershed transform (WT) [5], hidden Markov random field (HMRF) [6], fuzzy entropy [7], etc., are useful and popular due to their simplicity without depending on training samples and labels. In contrast to unsupervised image segmentation approaches, although some supervised approaches such as convolutional neural network (CNN) [8] and fully convolution networks (FCN) [9], are able to achieve image segmentation by using feature learning, but they require a lot of training samples and label images. In addition, the segmentation result has a coarse contour since CNN and FCN essentially achieve image classification. In this paper, we mainly discuss unsupervised image segmentation.

In unsupervised algorithms, clustering represents one kind of important and popular algorithms for grayscale and color image segmentation because it is suitable and useful for both low- and high-dimensional data. Generally, clustering algorithms can be roughly categorized into three groups—minimizing an objective function [10], decomposing a density function [11], and graph theory [12]. In this paper, we will focus on image segmentation based on clustering by minimizing an objective function. It is well-known that k-means and FCM are clustering algorithms by minimizing an objective function. Because k-means is a hard

T. Lei is with the School of Electronical and Information Engineering, Shaanxi University of Science and Technology, Xi'an 710021, China, and also with the School of Computer Science, Northwestern Polytechnical University, Xi'an 710072, China (e-mail: leitao@sust.edu.cn).

X. Jia is with the School of Electronical and Information Engineering, Shaanxi University of Science and Technology, Xi'an 710021, China (e-mail: jiaxhsust@163.com).

Y. Zhang is with the School of Computer Science, Northwestern Polytechnical University, Xi'an 710072, China (e-mail: ynzhang@nwpu.edu.cn).

S. Liu is with the School of Computer Science, Shaanxi Normal University, Xi'an 710119, China (e-mail: shgliu@gmail.com).

H. Meng is with the Department of Electronic and Computer Engineering, Brunel University London, Uxbridge UB8 3PH, U.K. (e-mail: hongying. meng@brunel.ac.uk).

A. K. Nandi is with the Department of Electronic and Computer Engineering, Brunel University London, Uxbridge UB8 3PH, U.K., and also with the Key Laboratory of Embedded Systems and Service Computing, College of Electronic and Information Engineering, Tongji University, Shanghai 200092, China (e-mail: asoke.nandi@brunel.ac.uk).

Color versions of one or more of the figures in this paper are available online at http://ieeexplore.ieee.org.

Digital Object Identifier 10.1109/TFUZZ.2018.2889018

clustering algorithm, it is sensitive to initial clustering centers or membership. In contrast, FCM is a soft algorithm that improves the shortcomings of *k*-means at the cost of increasing iterations. However, both *k*-means and FCM are sensitive to noise because the local spatial information of pixels is missed for image segmentation. To address this shortcoming, a great number of improved clustering algorithms that incorporate local spatial information into their objective function have been proposed in recent years [13]–[15]. These algorithms can be grouped into two groups. The first group employs neighborhood information of a center pixel using a window of fixed size to improve image segmentation effect, e.g., FCM algorithm with spatial constraints (FCM_S) [16], FCM_S1 [17], FCM_S2 [17], fast generalized FCM algorithm (FGFCM) [18], fuzzy local information c-means clustering algorithm (FLICM) [19], neighborhood weighted FCM clustering algorithm (NWFCM) [20], FCM algorithm based on noise detection (NDFCM) [21], Memon's algorithm [22], and the FLICM based on kernel metric and weighted fuzzy factor (KWFLICM) [23]. The advantage of these algorithms is that the neighborhood information can be computed in advance, except FCM_S and FLICM, to reduce the computational complexity. However, a neighborhood window of fixed size and shape is unable to satisfy the requirement of robust image segmentation. The second group employs adaptive neighborhood information instead of the window of fixed size and shape, e.g., Liu's algorithm [24], Bai's algorithm [25], and adaptive FLICM [26]. As adaptive neighborhood information is consistent with real image structuring information, the second group of algorithms obtains a better robustness for noisy images and a better segmentation effect than the first group.

Though improved FCM algorithms consider the neighborhood information of an image, the neighborhood information of the corresponding membership, which is helpful for improving classification effect, is ignored. HMRF [27]–[29] is a popular algorithm for addressing the issue. In [30], the current membership called posterior probability depends on clustering centers and the prior probability of neighborhood. Because HMRF considers the previous state of current membership, it obtains better result than FCM for image segmentation [30]. Based on the idea, Zhang *et al.* [31] incorporated the local spatial information of membership into the objective function of FCM, which obtains better results for image segmentation than the algorithm proposed in [30]. Furthermore, Liu *et al.* [24] improved FCM algorithm by integrating the distance between different regions obtained by mean-shift and the distance of pixels into its objective function. Although these HMRF-based clustering algorithms [24], [30], [31] effectively improve the effect of image segmentation, they have a high computational complexity caused by the computation of neighborhood information provided by original image and previous state's membership in every iteration.

It is clear that the algorithms mentioned above improve image segmentation effect at the cost of increasing the computational complexity. Therefore, the question arises how one can maintain local spatial information while reducing the computational complexity efficiently. Lei *et al.* [32] proposed a fast and robust FCM algorithm (FRFCM) to address the problem by employing morphological reconstruction [33] and membership filtering. Because the repeated distance computation between pixels

within neighborhood window and clustering centers is removed, the algorithm is very fast and provides a better segmentation result than state-of-the-art algorithms. Nevertheless, the FRFCM requires much execution time for color image segmentation because it is difficult to compute the histogram of color images. To address the issue, we propose a superpixel-based fast FCM (SF-FCM) for color image segmentation. The proposed algorithm is able to achieve color image segmentation with a very low computational cost, yet achieve a high segmentation precision.

Two contributions are presented as follows.

1) We present a multiscale morphological gradient reconstruction (MMGR) operation to generate superpixel image with accurate boundaries, which is helpful for integrating adaptive neighboring information and reducing the number of different pixels in a color image.
2) Based on a superpixel image obtained by MMGR, we propose a simple color histogram computational method that can be used to achieve a fast FCM algorithm for color image segmentation.

The rest of this paper is organized as follows. In Section II, we illustrate the motivation of our work. In Section III, we propose our model and analyze its superiority. The experimental results on synthetic images and real images are described in Section IV. Finally, we present our conclusion in Section V.

II. MOTIVATION

FCM often miss spatial information leading to a poor result for image segmentation. Although a great number of improved algorithms address the problem by incorporating local spatial information into the objective function, this, in turn, increases the computational complexity of algorithms. Fortunately, superpixel [34] is able to address the problem. Superpixel is an image preprocessing tool that oversegments an image into a number of small regions. A superpixel region is usually defined as perceptually uniform and homogenous regions in the image [35]. Superpixel is able to improve the effectiveness and efficiency of image segmentation due to two advantages. On the one hand, superpixel is able to achieve a presegmentation based on the local spatial information of images. The presegmentation provides better local spatial information than traditional neighboring windows employed by FCM_S, FLICM, FGFCM, KWFLICM, NWFCM, NDFCM, and FRFCM. On the other hand, superpixel is able to reduce the number of different pixels in an image by replacing all pixels in a region with the mean value of the superpixel region [36], [37]. In this paper, we will employ superpixel technology to obtain adaptive local spatial information, and then compute the histogram of superpixel image to achieve fast color image segmentation.

A. Motivation for Using Superpixel

In early improved FCM algorithms, local spatial information is often insufficient in a neighboring window of fixed size and shape. If the window is too small, the local spatial information will be limited for improving segmentation effect. But if the window is too large, the computational complexity of the corresponding algorithm will be very high. Recently, some improved FCM algorithms [26] incorporate adaptive local spatial information into their objective function to obtain better robustness

and higher performance for image segmentation. Adaptive local spatial information means that the pixels within a neighboring region have variable weighting factors depending on local characteristics of an image. For example, in Liu's algorithm [24], the adaptive neighborhood of a pixel is decided by its neighboring window and the corresponding region obtained by a prior mean-shift algorithm [11].

In [24], the objective function denoted by J_m is defined as

$$J_m = \sum_{i=1}^{N}\sum_{k=1}^{c} u_{ki}D_{ki} + \varpi \sum_{i=1}^{N}\sum_{k=1}^{c} u_{ki}\log\left(\frac{u_{ki}}{\pi_{ki}}\right) \quad (1)$$

where u_{ki} is the membership between the ith pixel and the kth clustering center, $1 \leq i \leq N$, $1 \leq k \leq c$, N is the number of data items, c is the number of clusters, $N, c \in N^+$, ϖ is the degree of fuzziness of u_{ki}, and the distance function D_{ki} is the combination of the pixel dissimilarity and region dissimilarity

$$D_{ki} = \frac{d_{ki} + d_{kR_i}}{2}. \quad (2)$$

In (2), d_{ki} is the dissimilarity distance between the ith pixel and the kth clustering center, d_{kR_i} is the region dissimilarity between the region R_i obtained by mean-shift and the kth clustering center, $d_{kR_i} = \frac{1}{\text{sum}(R_i)}\sum_{j \in R_i} d_{kj}$, R_i is the region that contains the ith pixel, and the $\text{sum}(R_i)$ denotes the number of pixels in the region R_i. Furthermore

$$\pi_{ki} = \frac{\sum_{j \in N_i} w_j \zeta_j u_{kj}}{\sum_{k=1}^{c}\sum_{j \in N_i} w_j \zeta_j u_{kj}}. \quad (3)$$

In (3), w_j is a weighting parameter of the neighborhood pixels, N_i is the neighborhood of the ith pixel, and $j \in N_i$, and ζ is the region-level iterative strength

$$\zeta_j = \frac{1}{Z}\left(E_{R_i, R_j} + 1\right)^{-1} \quad (4)$$

where $E_{R_i, R_j} = \|\text{mean}(R_i) - \text{mean}(R_j)\|$ is the Euclidean distance between the mean values of region R_i and R_j. $Z = \sum_{j \in N_i}\left(E_{R_i, R_j} + 1\right)^{-1}$ is a normalized constant.

Clearly, a prior oversegmentation obtained by mean-shift is necessary for Liu's algorithm. However, mean-shift is sensitive to parameters. Moreover, the fuzzy membership depends on both the pixel's neighboring window and the region containing the pixel.

Based on the analysis above, although Liu's algorithm is able to improve image segmentation effect by incorporating adaptive local spatial information into the objective function, it has a high computational complexity due to the repeated computation of adaptive neighboring information in every iteration. Although, we also employ adaptive neighboring information obtained by a superpixel algorithm to improve the segmentation effect, significantly different from Liu's algorithm is the fact that the proposed superpixel algorithm has a lower computational complexity.

B. Motivation for Using Histogram of Color Images

Traditional FCM algorithm has to compute the distance between each pixel and clustering centers, which leads to a high computational complexity when the resolution of an image is high. The enhanced FCM (EnFCM) proposed by Szilágyi *et al.* [38] solves the problem by performing clustering on gray levels instead of pixels. The idea is efficient for the reduction of the computational complexity because the repeated distance computation is removed by integrating histogram to its objective function. The objective function of EnFCM is defined as

$$J_m = \sum_{l=1}^{q}\sum_{k=1}^{c} \gamma_l u_{kl}^m \|f^l - v_k\|^2 \quad (5)$$

where u_{kl} represents the fuzzy membership of gray value l with respect to the kth clustering center v_k, m is the weighting exponent, f is a grayscale image, f^l is the gray level, $1 \leq l \leq q$, q denotes the number of the gray levels of f (it is generally far smaller than N), γ_l is the number of pixels whose gray level equals to f^l, and

$$\sum_{l=1}^{q} \gamma_l = N. \quad (6)$$

Clearly, the introduction of histogram is able to reduce the computational complexity of FCM. Because the level of histogram is far less than the number of pixels in an image, it is faster to implement FCM on gray levels than pixels for grayscale image segmentation. However, it is difficult to extend this idea of EnFCM to FCM for color image segmentation [39] because the number of different colors is usually close to the number of pixels in a color image. This is also the reason that FRFCM [32] usually requires a longer execution time to segment a color image than the corresponding grayscale image.

To address the issue, in this work, we will compute the histogram of a color image according to the corresponding superpixel image since the number of regions in the superpixel image is far smaller than the number of pixels in the original color image. We will use the mean value of all pixels within an area instead of these pixels to reduce the number of different colors in the original color image. It is easy to compute the histogram of the superpixel image because there is only a small number of different colors in the superpixel image. And then, the fast FCM algorithm will be achieved for color image segmentation, which will be presented in detail in Section III-B.

III. METHODOLOGY

Since a superpixel image is able to provide better local spatial information than a neighboring window of fixed size and shape, superpixel technologies such as mean-shift [11], simple linear iterative clustering (SLIC) [40], and WT [41], are usually considered as presegmentation algorithms for improving segmentation results generated by clustering algorithms [42], [43]. Compared to SLIC, mean-shift and WT produce irregular superpixel areas that are better than hexagonal regions obtained by SLIC. In practical applications, mean-shift is more popular than WT since the latter is sensitive to noise leading to a serious oversegmentation.

Even though mean-shift is able to provide better superpixel results, it is sensitive to parameter values, e.g., the spatial bandwidth denoted by h_s, the range bandwidth denoted by h_r, and the minimum size of final output regions denoted by h_k. Moreover, the computational complexity of mean-shift is higher than WT. Therefore, we need to develop a fast superpixel algorithm that can provide better presegmentation result and requires less time
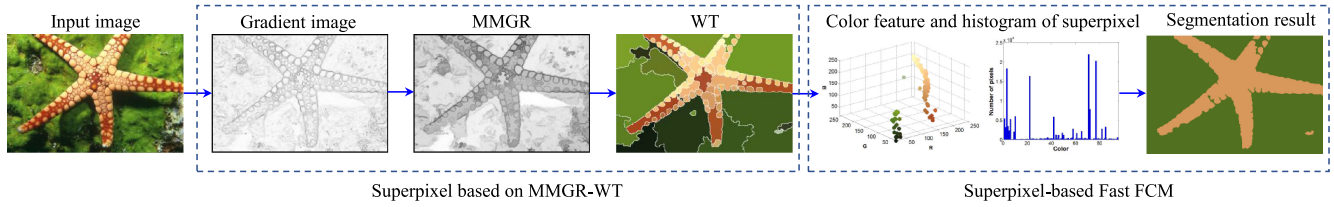
Fig. 1. Framework of the proposed algorithm.

than mean-shift. Because WT only depends on region minima of gradient images to obtain presegmentation, it has a very low computational complexity. In this work, we employ a novel WT based on MMGR (MMGR-WT) to produce superpixel images. The MMGR-WT is able to provide more appropriate presegmentation results using shorter execution time than mean-shift. Moreover, it is insensitive to parameters.

Based on the superpixel image obtained by MMGR-WT, we compute the histogram of superpixel images to achieve fast FCM algorithm. The computation of the histogram of superpixel images is easy because the number of different colors from superpixel images is far smaller than that from the original color image. Finally, the histogram is considered as a parameter of the objective function to achieve fast color image segmentation. The framework of our proposed algorithm is shown in Fig. 1.

A. Superpixel-Based on MMGR-WT

WT is a fast algorithm used for image segmentation via computing local minima of a gradient image and searching the watershed line between adjacent local minima. The algorithm easily causes an oversegmentation because it is sensitive to noise. To address the problem, many algorithms have been proposed by modifying the gradient image of the original image. Among these algorithms, morphological gradient reconstruction (MGR) [44] is a simple and efficient algorithm for overcoming oversegmentation because it is able to preserve the contour details of objects while removing noise and useless gradient details. First, the basic definition of morphological reconstruction is presented as follows:

$$\begin{cases} R_f^\varepsilon(g) = \varepsilon_f^{(i)}(g) \\ R_f^\delta(g) = \delta_f^{(i)}(g) \end{cases} \tag{7}$$

where R^ε and R^δ represent morphological erosion and dilation reconstruction, respectively, f is the original image, i.e., the mask image, g is the marker image, ε is the erosion operation, and δ is the dilation operation. Erosion reconstruction requires that $g \geq f$, but dilation reconstruction requires $g \leq f$, $\varepsilon_f^{(1)}(g) = \varepsilon(g) \vee f$, $\varepsilon_g^{(i)}(f) = \varepsilon(\varepsilon^{(i-1)}(g)) \vee f$, $\delta_f^{(1)}(g) = \delta(g) \wedge f$, and $\delta_g^{(i)}(f) = \delta(\delta^{(i-1)}(g)) \wedge f$. The symbols $\vee$ and $\wedge$ stand for the pointwise maximum and minimum, respectively.

Because morphological erosion and dilation are a pair of dual operators, they always appear in pairs such as morphological opening and closing operators. The morphological opening and closing are more popular than erosion and dilation because they have stronger capability for feature extraction or noise removal. Consequently, the morphological opening reconstruction denoted by R^O and closing reconstructions denoted by R^C, are
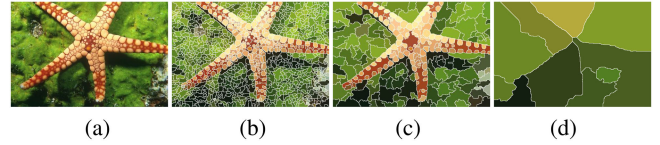

Fig. 2. Watershed segmentation based on MGR with different SEs. (a) Original image "12003" (image size: 481×321). (b) $r = 1$. (c) $r = 3$. (d) $r = 10$.

defined as

$$\begin{cases} R^O(g) = R^\delta(R^\varepsilon) \\ R^C(g) = R^\varepsilon(R^\delta) \end{cases} \tag{8}$$

where the marker image g is generally considered as $g = \varepsilon_B(f)$ in R^δ or $g = \delta_B(f)$ in R^ε. B is a structuring element (SE).

Both R^O and R^C are able to remove region minima in a gradient image to reduce oversegmentation. For instance, we use R^C to reduce oversegmentation as shown in Fig. 2.

In Fig. 2, the SE is defined as a disk, where r is the radius of the SE. Fig. 2 shows that the number of segmentation regions decreases quickly by increasing the value of r. However, a small SE easily leads to oversegmentation, while a large SE easily leads to undersegmentation. Therefore, it is difficult to obtain a superpixel image with both fewer regions and accurate contour by using MGR. To balance the number of regions in superpixel image and contour precision, a suitable SE is required, but it is difficult to choose a suitable SE for different images.

To solve the problem, we try to use different SEs to reconstruct a gradient image, and then fuse these reconstructed gradient images to remove the dependency of segmentation result on SEs. Thus, we propose a MMGR operation denoted by R^{MC} that is defined as follows:

$$R_f^{MC}(g, r_1, r_2) = \vee\{R_f^C(g)_{B_{r_1}}, R_f^C(g)_{B_{r_1+1}}, \ldots, R_f^C(g)_{B_{r_2}}\} \tag{9}$$

where r_1 and r_2 represent minimal and maximal r, respectively, $r_1 \leq r \leq r_2$, $r_1, r_2 \in N^+$, $g \leq f$.

We can see that R^{MC} employs multiscale SEs to reconstruct a gradient image to obtain multiple reconstructed images. By computing the pointwise maximum of these reconstructed gradient images, an excellent gradient image that removes most of useless local minima while preserving important edge details is obtained.

The proposed MMGR includes two parameters, r_1 and r_2, where r_1 controls the size of the minimal region and r_2 controls the size of the maximal region. If r_1 is too small, there will be many small regions in segmentation results, but if r_1 is too large, the boundary precision will be low. An example is shown in Fig. 3. It can be seen that the superpixel result has a high contour precision but includes some small regions

TABLE I
COMPARISON OF THE NUMBER OF SUPERPIXEL REGIONS FOR WT BASED ON MGR AND MMGR, RESPECTIVELY

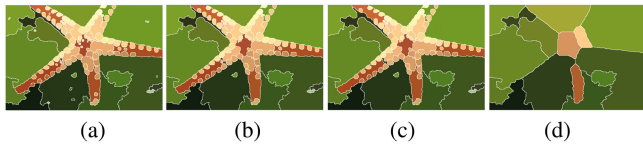|	MGR			MMGR		
Parameters	$r = 1$	$r = 3$	$r = 10$	$r_1 = 2, r_2 = 7$	$r_1 = 2, r_2 = 11$	$r_1 = 2, r_2 = 20$
Number	1210	263	10	264	95	95

Fig. 3. Segmentation results using MMGR-WT with different r_1, where $r_2 = 10$. (a) $r_1 = 1$. (b) $r_1 = 3$. (c) $r_1 = 5$, (d) $r_1 = 8$.
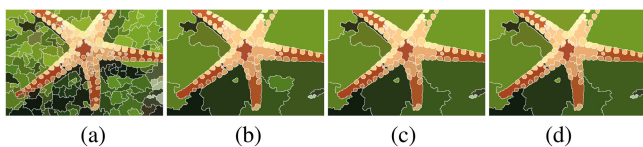

Fig. 4. Watershed segmentation based on MMGR-WT with different sized SEs. (a) $r_1 = 2, r_2 = 3$. (b) $r_1 = 2, r_2 = 7$. (c) $r_1 = 2, r_2 = 11$, (d) $r_1 = 2, r_2 = 20$.

when $r_1 = 1$, the superpixel result has a high contour precision and excludes small regions when $r_1 = 2$ or $r_1 = 3$, the superpixel result has a clearly low contour precision when $r_1 = 8$. Consequently, we choose $1 \leq r_1 \leq 3$ here. Because r_2 controls the size of the maximal region, the superpixel image is better when the value of r_2 is larger as shown in Fig. 4. However, the superpixel image is unchanged when the value of r_2 is larger than a threshold; for example, the threshold is 11 in Fig. 4. Clearly, the superpixel image is convergent via increasing the value of r_2. Moreover, the convergent result is perfect because it includes fewer regions and yet provides accurate contour. Therefore, the MMGR is insensitive to the change of r_2 when r_2 is larger than a threshold. Table I shows the comparison of the number of superpixel regions for WT-MGR and WT-MMGR, respectively.

r_2 can be a variant as can be seen from Table I. But it is difficult to set different values of r_2 for each image. In practical applications, r_2 is adaptive and it is not required for MMGR as long as we set a minimal error threshold denoted by η instead of r_2, i.e.,

$$\max \left\{ R_f^{MC}(g, r_1, r_2) - R_f^{MC}(g, r_1, r_2 + 1) \right\} \leq \eta. \quad (10)$$

In (10), r_2 can be replaced by η because r_2 is supposed to have different values for each image in a data set, but a fixed value of η can be used for all images in the data set. Note that if η is too large, r_2 will be small but the error will be large. On the contrary, if η is too small, the error will be small but r_2 will be large leading to a high computational burden for MMGR. Therefore, it is important to choose an appropriate η for a data set. We perform MMGR on ten images from the Berkeley segmentation dataset and benchmark (BSDS), we can obtain different values of r_2 according to a fixed value of η as shown in Table II.

Table II shows that the values of r_2 will be larger when decreasing η. However, r_2 will be unchanged when η is smaller or equal to 10^{-4}. Therefore, we set $\eta = 10^{-4}$ in this paper.

To demonstrate the effectiveness of the MMGR, Fig. 5 shows superpixel images obtained by SLIC, mean-shift, and MMGR-WT, respectively, where s_k is the number of desired superpixels, s_m is the weighting factor between color and spatial differences, and s_s is the threshold used for region merging. These parameters are selected depending on [40] and [42]. It can be seen from Fig. 5 that the superpixel images generated by SLIC include lots of areas with similar shape and size, but the superpixel images generated by the mean-shift and MMGR-WT include lots of areas with different shapes sizes. It is clear that later two algorithms provide better visual effect for the requirement of real images.

Although SLIC and mean-shift are able to generate superpixel images according to task requirements by changing parameters, they have a longer execution time than the proposed MMGR as shown in Table III, where SLIC corresponds to Fig. 5(b), mean-shift1 corresponds to Fig. 5(c), mean-shift2 corresponds to Fig. 5(d), and MMGR-WT corresponds to Fig. 5(e). Because our purpose is to propose a fast FCM algorithm for color image segmentation, MMGR is more appropriate than SLIC and mean-shift for our task requirement.

B. Superpixel-Based Fast Fuzzy c-Means

In Section III-A, we proposed the MMGR-WT to obtain better local spatial information used for fuzzy clustering. Because MMGR-WT depends on the local feature of an image, while FCM depends on the global feature, the combination of MMGR-WT and FCM is able to improve image segmentation result. In this section, we propose an SFFCM algorithm by incorporating adaptive local spatial information into the objective function of FCM.

EnFCM is popular and efficient for achieving fast image segmentation because a gray image only includes 256 gray levels, which is usually far smaller than the number of pixels in an image but the number of different colors in a color image is far larger than 256. The quantization technology is usually used to reduce the number of colors in an image. The basic idea of quantization technology is that a clustering algorithm is performed on each channel of a color image to obtain an image with fewer color levels than before. However, the traditional color quantization only reduces the number of different colors, but the color distribution of the quantized image is still similar to that of the original image because the local spatial information is ignored. Because a superpixel image carries the spatial information of the image and reduces the number of different colors, the superpixel image is superior to images quantized by clustering algorithms. We applied the clustering algorithm proposed in [39] and the proposed MMGR-WT to quantize a

TABLE II
VALUES OF r_2 FOR TEN IMAGES FROM BSDS FOR DIFFERENT VALUES OF η

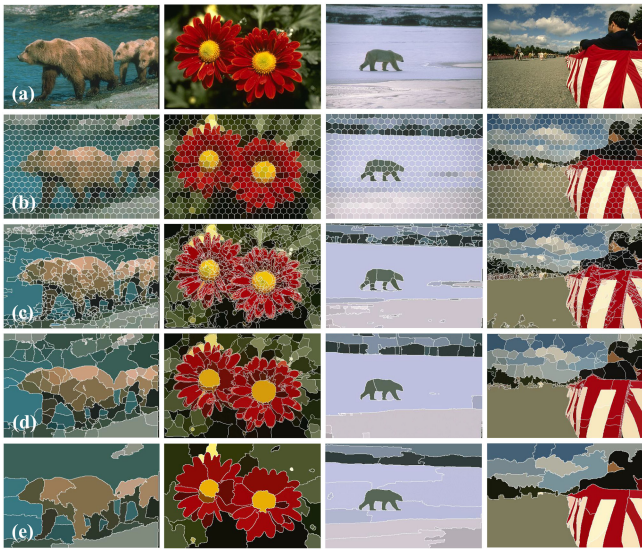| Images	$\eta = 10^{-2}$	$\eta = 10^{-3}$	$\eta = 10^{-4}$	$\eta = 10^{-5}$
"2092"	12	17	26	26
"3096"	10	10	10	10
"8023"	10	10	14	14
"8049"	14	19	22	22
"8143"	7	10	10	10
"12003"	12	18	18	18
"12074"	10	18	24	24
"12084"	14	15	15	15
"14037"	10	14	17	17
"15004"	14	18	18	18

Fig. 5. Superpixel images using different methods. (a) Original images. (b) Superpixel images obtained by SLIC ($s_k = 500$, $s_m = 50$, $s_s = 1$). (c) Superpixel images obtained by mean-shift1 with $h_s = 7$, $h_r = 7$, $h_k = 30$. (d) Superpixel images obtained by mean-shift2 with $h_s = 15$, $h_r = 15$, $h_k = 50$. (e) Superpixel images obtained by MMGR-WT ($r_1 = 2$).

TABLE III
COMPARISON OF EXECUTION TIME (IN SECONDS) OF DIFFERENT METHODS
USED TO GENERATE SUPERPIXEL IMAGES

Algorithms	"100075"	"124084"	"100007"	"145086"	Average
SLIC	3.86	4.07	3.89	3.88	3.93
mean-shift1	1.02	1.22	0.94	1.20	1.10
mean-shift2	2.66	1.22	2.67	2.86	2.79
MMGR-WT	**0.32**	**0.32**	**0.31**	**0.36**	**0.33**

The best values are in bold.

color image, and then computed the histogram of the quantized image as shown in Fig. 6, where the number of different colors is 57 214 in the original image. Furthermore, Fig. 7, the color distribution of Fig. 6, shows that the proposed MMGR-WT is more appropriate than clustering algorithm proposed in [39] for subsequent image segmentation.

It is clear that the histograms of Fig. 6(b) and (d) are simpler with only a small number of different colors appearing in the quantized images. According to Fig. 6(c) and (e), we can ex-
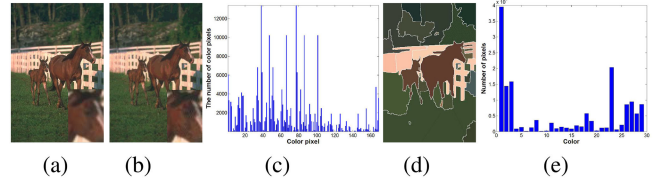

Fig. 6. Quantization of a color image and the corresponding histogram. (a) Original image. (b) Color quantization using the algorithm proposed in [39] ($c = 10$). (c) Histogram of Fig. 1(b). (d) Superpixel image using MMGR-WT ($r_1 = 2$). (e) Histogram of Fig. 1(c).
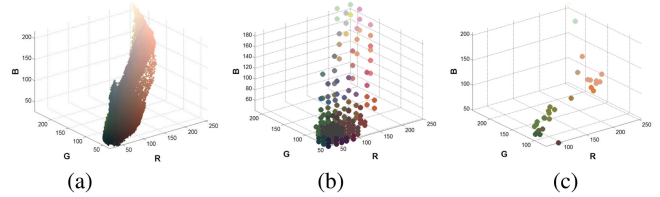

Fig. 7. Color distribution of different color images. (a) Color distribution of Fig. 6(a). (b) Color distribution of Fig. 6(b). (c) Color distribution of Fig. 6(d).

tend EnFCM to color image segmentation easily. Compared to Fig. 6(c), Fig. 6(e) has even fewer color levels. In addition, it is clear that the color distributions of Fig. 7(c) is different from Fig. 7(a) and (b), and the former is helpful for subsequent pixel classification.

Based on the superpixel image obtained by MMGR-WT, we proposed the objective function of SFFCM for color image segmentation as follows:

$$J_m = \sum_{l=1}^{q} \sum_{k=1}^{c} S_l u_{kl}^m \left\| \left(\frac{1}{S_l} \sum_{p \in R_l} x_p \right) - v_k \right\|^2 \quad (11)$$

where l is the color level, $1 \leq l \leq q$, q is the number of regions of the superpixel image, $l, q \in N^+$, S_l is the number of pixels in the lth region R_l, and x_p is the color pixel within the lth region of the superpixel image obtained by MMGR-WT. The new objective function only introduces histogram information compared with the old one in FCM. Because each color pixel in the original image is replaced by the mean value of color pixels within the corresponding region of the superpixel image, the number of color level is equivalent to the number of regions in the superpixel image. Thus, the computational complexity is efficiently reduced due to $l \ll N$.

Utilizing the Lagrange multiplier technique, the aforementioned optimization problem can be converted to an unconstrained optimization problem that minimizes the following objective function, i.e.,

$$\widetilde{J}_m = \sum_{l=1}^{q} \sum_{k=1}^{c} S_l u_{kl}^m \left\| \left(\frac{1}{S_l} \sum_{p \in R_l} x_p \right) - v_k \right\|^2 - \lambda \left(\sum_{k=1}^{c} u_{kl} - 1 \right) \quad (12)$$

where λ is a Lagrange multiplier. We compute the partial differential equation of $\widetilde{J}_m$ with respect to u_{kl} and v_k,

respectively

$$
\frac{\partial \widetilde{J}_m}{\partial u_{kl}} = \sum_{l=1}^{q} \sum_{k=1}^{c} \frac{\partial S_l u_{kl}^m \left\| \left(\frac{1}{S_l} \sum_{p \in R_l} x_p \right) - v_k \right\|^2}{\partial u_{kl}} - \lambda
$$

$$
= \sum_{l=1}^{q} \sum_{k=1}^{c} m S_l u_{kl}^{m-1} \left\| \left(\frac{1}{S_l} \sum_{p \in R_l} x_p \right) - v_k \right\|^2 - \lambda
$$

$$
= 0 \tag{13}
$$

$$
\frac{\partial \widetilde{J}_m}{\partial v_k} = \sum_{l=1}^{q} \sum_{k=1}^{c} \frac{\partial S_l u_{kl}^m \left\| \left(\frac{1}{S_l} \sum_{p \in R_l} x_p \right) - v_k \right\|^2}{\partial v_k}
$$

$$
= \sum_{l=1}^{q} \sum_{k=1}^{c} S_l u_{kl}^m \frac{\partial \left\| \left(\frac{1}{S_l} \sum_{p \in R_l} x_p \right) - v_k \right\|^2}{\partial v_k}
$$

$$
= \sum_{l=1}^{q} S_l u_{kl}^m \frac{\partial \left\| \left(\frac{1}{S_l} \sum_{p \in R_l} x_p \right) - v_k \right\|^2}{\partial v_k}
$$

$$
= -2 \sum_{l=1}^{q} S_l u_{kl}^m \left\| \left(\frac{1}{S_l} \sum_{p \in R_l} x_p \right) - v_k \right\|
$$

$$
= 0. \tag{14}
$$

Combing (13) and (14) together, the corresponding solutions for u_{kl} and v_k are obtained as

$$
v_k = \frac{\sum_{l=1}^{q} u_{kl}^m \sum_{p \in R_l} x_p}{\sum_{l=1}^{q} S_l u_{kl}^m} \tag{15}
$$

$$
u_{kl} = \frac{\left\| \left(\frac{1}{S_l} \sum_{p \in R_l} x_p \right) - v_k \right\|^{-2/(m-1)}}{\sum_{j=1}^{c} \left\| \left(\frac{1}{S_l} \sum_{p \in R_l} x_p \right) - v_j \right\|^{-2/(m-1)}}. \tag{16}
$$

Based on (9)–(16), the proposed SFFCM algorithm can be summarized as follows.

Step 1: Set values for c, m, r_1, η, η', where η' is the convergence condition used for SFFCM.

Step 2: Compute a superpixel image using (9)–(10), and then compute its histogram.
   1) Compute the gradient image using Sobel operators.
   2) Implement MMGR using (9)–(10) and η.
   3) Implement WT to obtain the superpixel image.

Step 3: Initialize randomly the membership partition matrix $\boldsymbol{U}^{(O)}$ according to the superpixel image.

Step 4: Set the loop counter $b = 0$.

Step 5: Update the clustering centers using (15).

Step 6: Update the membership partition matrix $\boldsymbol{U}^{(t)}$ using (16).

Step 7: If $\max\{\boldsymbol{U}^{(b)} - \boldsymbol{U}^{(b+1)}\} < \eta'$ then stop, otherwise, set $b = b + 1$ and go to Step 5.

We applied the proposed SFFCM to Fig. 6(a) following the previous steps. Then, the segmentation result is shown in Fig. 8. We can see that the proposed SFFCM is able to obtain better
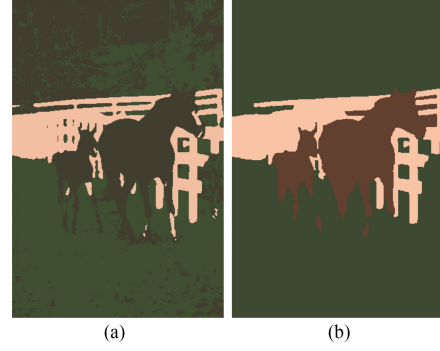

(a) (b)

Fig. 8. Segmentation results on Fig. 6(a). (a) Segmentation result using FCM for quantized image. (b) Segmentation result using the proposed SFFCM.

segmentation result than the traditional algorithm. Based on the analysis mentioned above, we conclude that the proposed SFFCM has following advantages.
   1) SFFCM is very fast for color image segmentation because the number of different colors is reduced efficiently due to superpixel and color histogram.
   2) SFFCM is insensitive to the change of parameters because the superpixel image obtained by MMGR-WT is convergent.
   3) SFFCM obtains an excellent result for color image segmentation because both adaptive local spatial information and global color feature are incorporated into the objective function.

IV. EXPERIMENTS

We conduct experiments on two synthetic color images of size 256×256 and real color images from the BSDS [45] and the Microsoft Research Cambridge (MSRC) [46]. The first synthetic image includes four different colors, while the second includes five different colors. The experiments are conducted on a DELL desktop with Intel Core CPU, i7-6700, 3.4 GHz, 16 GB RAM.

A. Comparative Algorithms

To assess the effectiveness and efficiency of the proposed SFFCM, nine comparative algorithms based on clustering used for color image segmentation are presented, i.e., FCM [10], FGFCM [18], HMRF-FCM [30], FLICM [19], NWFCM [20], KWFLICM [23], NDFCM [21], Liu's algorithm [24], and FR-FCM [32]. Since these algorithms employ different local spatial neighborhoods to improve segmentation results, they have different advantages and disadvantages.

B. Parameters Setting

Since both comparative algorithms and the proposed SFFCM belong to clustering algorithms based on objective function optimization, three indispensable parameters: the weighting exponent, the convergence condition, and the maximal number of iteration must be set before iterations. In our experiments, the three parameters are 2, 10^{-5}, and 50, respectively. In addition, the value of the minimal error threshold used for MMGR is 10^{-4}. In the comparative algorithms, a window of size 3×3 is employed by those algorithms required a neighboring window
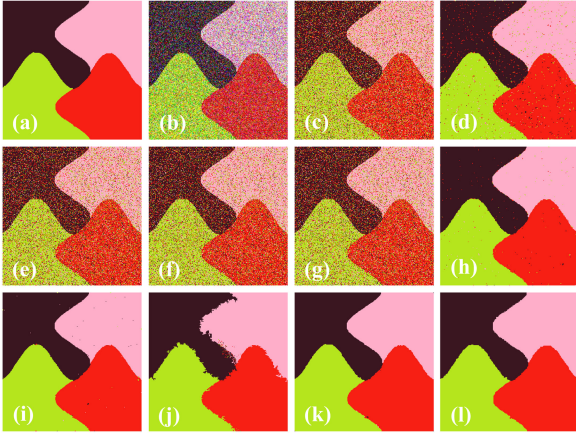
Fig. 9.   Comparison of segmentation results on the first symmetric image. (a) First synthetic image. (b) Noisy image (Gaussian noise, the noise level is 10%). (c) FCM. (d) FGFCM. (e) HMRF-FCM. (f) FLICM. (g) NWFCM. (h) KWFLICM. (i) NDFCM. (j) Liu's algorithm. (k) FRFCM. (l) SFFCM.
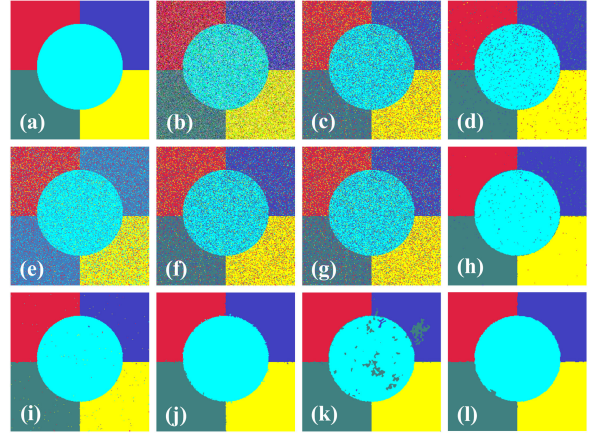

Fig. 10.   Comparison of segmentation results on the second symmetric image. (a) Second synthetic image. (b) Noisy image (Salt & Pepper, the noise level is 40%). (c) FCM. (d) FGFCM. (e) HMRF-FCM. (f) FLICM. (g) NWFCM. (h) KWFLICM. (i) NDFCM. (j) Liu's algorithm. (k) FRFCM. (l) SFFCM.

of fixed size for fair comparison. Moreover, the computational complexity is also an important reason for the choice of the window of size 3×3. In addition, a neighborhood window is unnecessary for FCM. According to the criterion of parameters setting mentioned in those comparative algorithms, the spatial scale factor and the gray-level scale factor in FGFCM and ND-FCM, are $\lambda_s = 3$ and $\lambda_g = 5$, respectively. The third parameter of the NDFCM, a new scale factor is $\lambda_a = 3$. The NWFCM only refers to the gray-level scale factor, $\lambda_g = 5$. Because Liu's algorithm requires a presegmentation obtained by mean-shift, three parameters $h_s = 10$, $h_r = 10$, and $h_k = 100$ follow the original paper. Except three indispensable parameters mentioned above and the number of the cluster prototypes, HMRF-FCM, FLICM, and KWFLICM do not require any other parameters. In FRFCM, the SE used for multivariate morphological reconstruction is a square of size 3×3, and the filtering window used for membership filtering is also a square of size 3×3. As the proposed SFFCM needs a minimal SE for MMGR, we set $r_1 = 2$ for MMGR.

C. Results on Synthetic Images

First, we test these comparative algorithms and the proposed SFFCM on two synthetic color images to show their robustness to noise. In this experiment, three kinds of different noise Gaussian, Salt & Pepper, and Uniform noise are added to these synthetic images. All algorithms mentioned above are implemented and segmentation results are shown in Fig. 9 and 10.

FCM, HMRF-FCM, FLICM, and NWFCM provide poor results as shown in Figs. 9(c), (e), (f), and (g) and 10(c), (e), (f), and (g), which show that they are sensitive to both Gaussian and Salt & Pepper noise. HMRF-FCM, FLICM, and NWFCM cannot improve the FCM algorithm for color images. FGFCM, ND-FCM, and FRFCM obtain good segmentation results as shown in Fig. 9(d), (i), and (k) for the image corrupted by Gaussian noise, but poor segmentation results as shown in Fig. 10(d), (i), and (k) for the image corrupted by Salt & Pepper noise. It is clear that the three algorithms are insensitive to Gaussian noise but they are sensitive to Salt & Pepper noise of high density. KWFLICM, Liu's algorithm, and the proposed SFFCM pro-

vide better results as shown in Figs. 9(h), (j), and (l) and 10(h), (j), and (l), which demonstrates that they are robust against both Gaussian noise and Salt & Pepper noise as adaptive neighboring information is employed by the three algorithms.

To assess the performance of different algorithms on noisy image segmentation, two performance indices, the quantitative score (S) that is the degree of equality between pixel sets A_k and the ground truth (GT) C_k and the optimal segmentation accuracy (SA) that is the sum of the correctly classified pixels divided by the sum of the total number of the pixels [23], are adopted. S and SA are defined as

$$S = \sum_{k=1}^{c} \frac{A_k \bigcap C_k}{A_k \bigcup C_k} \tag{17}$$

$$\mathrm{SA} = \sum_{k=1}^{c} \frac{A_k \bigcap C_k}{\sum_{j=1}^{c} C_j} \tag{18}$$

where A_k is the set of pixels belonging to the kth class found by the algorithm, while C_k is the set of pixels belonging to the class in the GT. We implemented each of these algorithms on two synthetic images, and computed the mean value and the root mean square error (RMSE) of S and SA as shown in Tables IV and V.

In Tables IV and V, FCM, HMRF-FCM, FLICM, and NWFCM obtain similar S values as well as SA values, which further demonstrates that HMRF-FCM, FLICM, and NWFCM are inefficient for color image segmentation. FCM misses the local spatial information leading to poor segmentation result. HMRF-FCM, FLICM, and NWFCM only employ a small neighboring window to incorporate local spatial information into their objective function, which is helpful for segmenting images corrupted by low-density noise but not useful for segmenting images corrupted by high-density noise. FGFCM and NDFCM obtain higher values of S and SA than FCM, HMRF-FCM, FLICM, and NWFCM because the tested images are synthetic and the added noise is known. Because FGFCM and NDFCM employ a filter to suppress noise before iterations in clustering, they obtain larger S and SA than FCM, HMRF-FCM, FLICM, and NWFCM for synthetic images corrupted by known noise.

TABLE IV
COMPARISON SCORES (S%) OF THE TEN ALGORITHMS ON THE FIRST SYNTHETIC IMAGE CORRUPTED BY NOISE OF DIFFERENT LEVELS ($c = 4$)

Noise	FCM	FGFCM	HMRF-FCM	FLICM	NWFCM	KWFLICM	NDFCM	Liu's algorithm	FRFCM	SFFCM
Gaussian 5%	95.53	99.85	95.60	95.60	95.61	99.78	99.87	99.41	99.82	99.20
Gaussian 10%	85.69	99.75	85.70	85.69	85.70	99.68	99.61	98.46	99.81	99.17
Gaussian 15%	66.35	98.20	66.24	66.26	66.25	99.24	99.50	97.54	99.62	99.15
Gaussian 20%	55.22	94.05	55.29	55.31	55.29	98.45	99.53	96.76	99.48	98.98
Salt & Pepper 10%	80.21	95.56	80.21	80.21	80.21	99.65	81.91	99.67	99.68	99.18
Salt & Pepper 20%	65.54	87.55	65.54	65.54	65.54	98.66	71.28	99.23	98.58	98.91
Salt & Pepper 30%	51.51	77.21	54.07	54.07	54.07	95.21	69.39	98.55	97.11	98.68
Salt & Pepper 40%	42.19	65.94	44.51	42.19	44.51	87.69	66.60	96.76	78.64	92.83
Uniform 10%	84.41	99.49	84.44	84.41	84.45	99.81	82.31	99.77	99.81	99.22
Uniform 20%	71.08	97.95	71.02	71.08	71.02	99.57	77.59	99.28	99.68	99.19
Uniform 30%	59.83	94.31	60.00	60.08	60.00	98.91	89.23	98.72	99.39	98.99
Uniform 40%	50.05	87.46	49.94	50.05	49.94	96.50	99.46	97.23	98.44	98.83
Mean value	67.30	91.44	67.71	67.54	67.72	97.76	86.36	98.45	97.51	**98.53**
RMSE	16.49	10.48	15.98	16.28	15.98	3.48	13.15	**1.11**	6.00	1.80

The best values are in bold.

TABLE V
SA (SA%) OF TEN ALGORITHMS ON THE SECOND SYNTHETIC IMAGE CORRUPTED BY NOISE OF DIFFERENT LEVELS ($c = 5$)

Noise	FCM	FGFCM	HMRF-FCM	FLICM	NWFCM	KWFLICM	NDFCM	Liu's algorithm	FRFCM	SFFCM
Gaussian 3%	93.10	99.43	93.09	93.10	93.10	99.47	99.87	99.96	99.64	99.59
Gaussian 5%	87.03	98.44	86.85	87.01	86.86	99.04	99.70	99.96	99.55	99.52
Gaussian 10%	74.71	95.74	74.24	74.64	74.33	97.52	99.52	98.58	97.09	99.38
Gaussian 15%	66.02	92.30	65.70	66.06	65.70	95.69	98.84	97.09	94.87	99.41
Salt & Pepper 10%	86.42	97.33	86.46	86.42	73.86	99.44	91.26	99.84	99.57	99.55
Salt & Pepper 20%	74.40	92.41	74.54	74.40	74.54	98.55	89.52	99.68	97.08	99.48
Salt & Pepper 30%	63.52	84.59	58.15	63.52	58.15	95.59	86.49	99.03	92.60	99.00
Salt & Pepper 40%	49.86	75.76	48.89	49.86	48.89	76.97	62.54	97.56	85.48	98.99
Uniform 10%	90.41	99.26	90.38	90.42	90.38	99.47	94.13	99.91	99.62	99.59
Uniform 20%	81.09	97.77	80.97	81.09	80.97	99.16	90.17	99.81	98.95	99.53
Uniform 30%	72.34	94.96	62.67	72.34	72.02	98.13	99.59	99.64	96.71	99.41
Uniform 40%	63.42	89.73	62.80	63.42	54.73	82.16	99.82	82.75	93.71	99.20
Mean value	75.19	93.14	73.73	75.19	72.79	95.10	96.62	97.81	96.24	**99.39**
RMSE	13.01	7.02	14.16	13.01	14.00	7.46	10.67	4.84	4.17	**0.21**

The best values are in bold.

FRFCM obtains high S and SA when noisy density is low, but small S and SA when noisy density is high because FRFCM employ multivariate morphological reconstruction to simplify image and use the membership filtering to improve segmentation results.

As KWFLICM, Liu's algorithm, and the proposed SFFCM employ adaptive local spatial information to improve segmentation results, they obtain larger S and SA than those comparative algorithms that employ local spatial information in a window of fixed size. Liu's algorithm obtains higher values of S and SA because of the combination of mean-shift, FCM, and HMRF. In some cases, the proposed SFFCM provides smaller S and SA than Liu's algorithm but higher values than those comparative algorithms because contour details are smoothed in segmentation results obtained by the SFFCM. However, SFFCM provides the best mean value of S for two synthetic images and the best RMSE of SA for the second synthetic image, which shows that SFFCM is able to obtain good segmentation results for images corrupted by different noises.
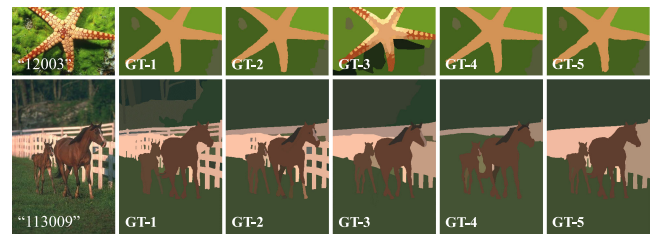

Fig. 11.   GT segmentations of images "12003" and "113009" from BSDS.

D. Results on Real Images

To demonstrate that the proposed SFFCM is useful for real image segmentation, we further conducted experiments on the BSDS and MSRC. The BSDS is a popular benchmark that has been widely used by researchers for the task of image segmentation [45]. The early BSDS is named as BSDS300 that is composed of 300 images and the current BSDS is an extended
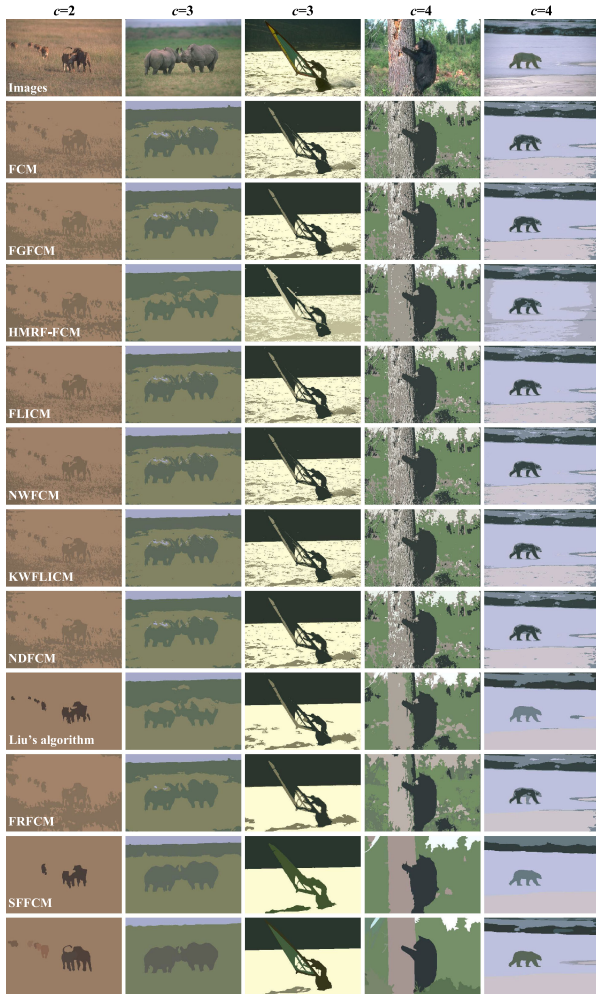
Fig. 12. Comparison of segmentation results on color images from BSDS using different models.

Fig. 13. Comparison of segmentation results on color images from BSDS using different models.

version that is composed of 500 images, called BSDS500. For each image in BSDS, there are four to nine GT segmentations. These GT segmentations are delineated by different human subjects. For instance, there are five GT segmentations delineated by five subjects on image "12003" and "113009" as shown in Fig. 11. The MSRC data set contains 23 object classes and comprises of 591 natural images. For each image in MSRC, there is only one GT segmentation that is pixel-wise labeled.

Figs. 12–14 show segmentation results of images from the BSDS and MSRC. The parameters setting is the same as that in Section IV-B. Since the size of images in BSDS and MSRC is different from the size of synthetic images, the SE used for multivariate morphological reconstruction in FRFCM is a disk of size 5×5 for the BSDS and MSRC. The value of r_1 is set to 3 for real images in this section. In addition, the CIE-Lab color space is used for all algorithms for fair comparison.

As can be seen from Figs. 12 and 13, segmentation results obtained by FCM, FGFCM, HMRF-FCM, FLICM, NWFCM, KWFLICM, and NDFCM include a great number of small regions because only a small local neighboring window is employed (a large neighboring window will cause a very high computational complexity). FRFCM obtains better results than
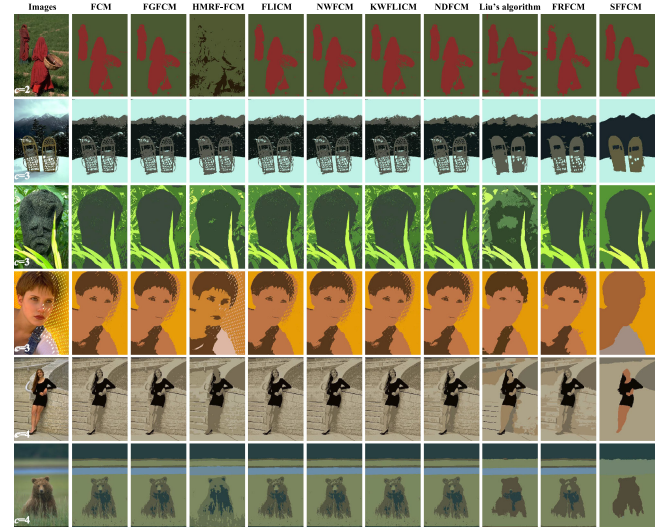
algorithms mentioned above due to the introduction of multivariate morphological reconstruction and membership filtering. However, Liu's algorithm and the proposed SFFCM obtain better results than FRFCM due to the use of adaptive local spatial information provided by presegmentation. Although Liu's algorithm provides a better segmentation result than the proposed SFFCM on the left image, the later provides better results than the former on four other images in Fig. 12. In practical applications, since it is difficult to propose an algorithm to achieve the best segmentation result for every image in a data set, researchers usually use the average result on all images in the data set, e.g., BSDS and MSRC, to estimate the algorithm performance.

In Fig. 14, all algorithms are efficient for images in which the foreground is clearly different from the background as shown in the first row. A large number of small regions appear in segmented images except images obtained by SFFCM as shown in the second to fifth rows. Liu's algorithm, FRFCM, and SFFCM obtain better results than other algorithms as shown in the sixth row. All algorithms fail to segment images except SFFCM, as shown in the last three rows.

To evaluate segmentation results obtained by different algorithms, five performance measures [45], [47], namely, the probabilistic rand index (PRI), the covering (CV), the variation of information (VI), the global consistency error (GCE), and the boundary displacement error (BDE), are computed in this experiment. The PRI is a similarity measure that counts the fraction of pairs of pixels whose labels are consistent between the computed segmentation and the corresponding GT segmentation. The CV is an overlap measure that can be also used to evaluate the segmentation effect. The VI is a similarity measure that is always used to measure the distance between two segmentations in terms of their average conditional entropy. The GCE computes the degree to which two segmentations are mutually consistent. The BDE is an error measure that is used to measure the average displacement error of boundary pixels between two segmentations. If the segmentation result is more similar to the GT, PRI and CV will be larger but VI, GCE, and BDE will be smaller. In the BSDS, each image corresponds to

Fig. 14. Comparison of segmentation results on color images from MSRC using different models ($c = 2$).

TABLE VI
AVERAGE PERFORMANCE OF TEN ALGORITHMS ON THE BSDS300 THAT
INCLUDES 300 IMAGES

Algorithms	PRI↑	CV↑	VI↓	GCE↓	BDE↓
FCM	0.74	0.43	2.87	0.41	13.78
FGFCM	0.74	0.43	2.80	0.40	13.63
FLICM	0.74	0.43	2.82	0.40	13.69
NWFCM	0.74	0.43	2.78	0.41	13.78
KWFLICM	0.74	0.43	2.82	0.40	13.70
NDFCM	0.74	0.44	2.87	0.39	13.52
HMRF-FCM	0.74	0.43	2.77	0.40	13.71
Liu's algorithm	0.77	0.48	2.53	0.35	**12.57**
FRFCM	0.75	0.46	2.62	0.36	12.87
SFFCM	**0.78**	**0.55**	**2.02**	**0.26**	12.90

The best values are in bold.

TABLE VIII
AVERAGE PERFORMANCE OF TEN ALGORITHMS ON THE MSRC THAT
INCLUDES 591 IMAGES

Algorithms	PRI↑	CV↑	VI↓	GCE↓	BDE↓
FCM	0.70	0.55	1.93	0.32	12.67
FGFCM	0.70	0.56	1.85	0.31	12.39
FLICM	0.72	0.59	1.73	0.28	12.29
NWFCM	0.69	0.55	1.90	0.32	12.61
KWFLICM	0.69	0.55	1.93	0.32	12.67
NDFCM	0.69	0.55	1.90	0.32	12.54
HMRF-FCM	0.70	0.56	1.84	0.31	12.38
Liu's algorithm	0.71	0.54	1.77	0.34	12.43
FRFCM	0.71	0.58	1.79	0.30	**12.23**
SFFCM	**0.73**	**0.62**	**1.58**	**0.25**	12.49

The best values are in bold.

TABLE VII
AVERAGE PERFORMANCE OF TEN ALGORITHMS ON THE BSDS500 THAT
INCLUDES 500 IMAGES

Algorithms	PRI↑	CV↑	VI↓	GCE↓	BDE↓
FCM	0.74	0.43	2.88	0.40	13.48
FGFCM	0.75	0.44	2.81	0.39	13.28
FLICM	0.74	0.43	2.83	0.40	13.38
NWFCM	0.74	0.43	2.88	0.40	13.47
KWFLICM	0.74	0.44	2.83	0.40	13.40
NDFCM	0.75	0.44	2.78	0.39	13.13
HMRF-FCM	0.75	0.43	2.78	0.40	13.22
Liu's algorithm	0.76	0.47	2.58	0.36	**12.31**
FRFCM	0.76	0.45	2.67	0.37	12.35
SFFCM	**0.78**	**0.54**	**2.06**	**0.26**	12.80

The best values are in bold.

TABLE IX
AVERAGE PERFORMANCE OF SFFCM ON BSDS300

Exponent	PRI↑	CV↑	VI↓	GCE↓	BDE↓
$m = 2$	0.78	0.55	2.02	0.26	12.90
$m = 5$	0.78	0.55	2.00	0.26	12.91
$m = 10$	0.78	0.55	2.01	0.25	12.87
$m = 30$	0.78	0.55	2.02	0.26	13.03
$m = 100$	0.78	0.55	2.01	0.25	12.89

TABLE X
AVERAGE PERFORMANCE OF SFFCM ON BSDS500

Exponent	PRI↑	CV↑	VI↓	GCE↓	BDE↓
$m = 2$	0.78	0.54	2.06	0.26	12.80
$m = 5$	0.78	0.54	2.04	0.26	12.72
$m = 10$	0.78	0.54	2.06	0.26	12.72
$m = 30$	0.78	0.54	2.06	0.26	13.80
$m = 100$	0.78	0.54	2.05	0.26	12.82

TABLE XI
COMPARISON OF EXECUTION TIMES (IN SECONDS) OF TEN ALGORITHMS

	FCM	FGFCM	HMRF-FCM	FLICM	NWFCM	KWFLICM	NDFCM	Liu's algorithm	FRFCM	SFFCM
The first image	0.48	1.65	43.31	57.88	48.45	64.46	4.62	23.49	0.69	**0.19**
The second image	0.87	2.06	47.43	121.05	80.39	133.9	4.82	23.69	0.91	**0.21**
BSDS500	1.15	4.67	73.43	195.53	136.20	206.70	11.26	79.88	1.87	**0.74**
MSRC	**0.22**	1.59	19.35	37.76	30.07	39.83	4.60	17.75	0.53	0.29

The best values are in bold.

multiple GT segmentations, which leads to a result that a segmentation result corresponds to multiple groups of performance index. Therefore, the average value of multiple groups of performance index is usually considered as the final performance index of the segmentation result.

All these algorithms are evaluated on the BSDS and MSRC data sets. The value of c is set from 2 to 6 for each image in the BSDS, while its value is set from 2 to 4 for each image in the MSRC. We choose the best value of c corresponding to the highest PRI. Because the BSDS and MSRC includes lots of images, the average values of PRI, CV, VI, GCE, and BDE corresponding to segmentation results of all images in the BSDS or MSRC are presented in Tables VI–VIII. In Tables VI–VII, we can see that FCM, FGFCM, FLICM, NWFCM, and KWFLICM have similar values of the PRI, CV, VI, GCE, and BDE. NDFCM has the similar performance with HMRF-FCM. FRFCM clearly outperforms other algorithms on PRI and BDE due to the introduction of multivariate morphological reconstruction. Liu's algorithm obtains better performance than FRFCM because it computes the distance between pixels and clustering centers according to the combination of superpixel image and the original image. Similarly, Table VIII shows that FLICM, NWFCM, and KWFLICM have similar values of the PRI, CV, VI, GCE, and BDE. The performance of FGFCM is similar to NDFCM. Different from Tables VI–VII, HMRF-FCM obtains better performance than Liu's algorithm and FRFCM as shown in Table VIII. Clearly, the proposed SFFCM is the most excellent because it obtains the best values of PRI, CV, VI, and GCE, as well as within the 0.04 of the best value obtained of BDE as shown in Tables VI–VIII and the best segmentation results as shown in Figs. 12–14.

To demonstrate that the proposed SFFCM is insensitive to parameters, we further discussed the relationship between the weighting exponent m and the SFFCM. We have known that FCM algorithm is insensitive to m when the FCM is used for image segmentation. The proposed SFFCM has the same objective function with FCM. The difference between them is that the proposed SFFCM employ color histogram created by MMGR-WT to speed up the FCM algorithm. Therefore, theoretically, the performance of the proposed SFFCM is also insensitive to the value of m. Tables IX and X show the performance of SFFCM for different values of m. Fig. 15 shows the plot of Tables IX and X. It is clear that the performance of SFFCM is changed slightly via changing the value of m.

E. Execution Time

Execution time is an important index used to measure the performance of an algorithm. Table XI shows execution time of different algorithms on two synthetic images and real images
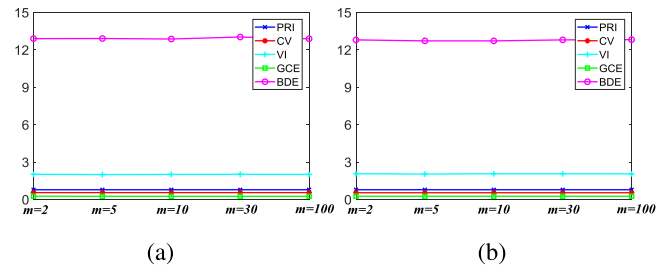

Fig. 15. Plot corresponding to Tables IX and X. (a) BSDS300. (b) BSDS500.

used in Sections IV-C–IV-D. We computed the average execution time of algorithms on images from the BSDS and MSRC, respectively.

It can be seen from Table XI that FCM is faster than other algorithms, except SFFCM, because no additional computation is implemented. FGFCM and NDFCM are faster than FLICM, NWFCM, and KWFLICM because the neighboring information is computed in advance. FLICM, NWFCM, and KWFLICM repeatedly compute the neighboring information in each iteration leading to a high computational complexity. Both HMRF-FCM and Liu's algorithm require a long execution time because a prior probability used for HMRF model must be computed in each iteration. FRFCM is fast because multivariate morphological reconstruction and membership filtering are implemented only once. The proposed SFFCM is very fast even faster than FCM for some images because the number of different colors in superpixel image obtained by MMGR-WT is decreased efficiently and the color histogram is integrated into SFFCM.

V. CONCLUSION

In this paper, an SFFCM algorithm for color image segmentation has been proposed. Two main contributions are presented. The first contribution is that we presented the MMGR operation to obtain a good superpixel image. The second contribution is that we incorporated color histogram into objective function to achieve fast image segmentation. The proposed SFFCM is tested on synthetic and real images. The experimental results demonstrate that the proposed SFFCM is superior to state-of-the-art clustering algorithms because it provides the best segmentation results and requires the shortest running time.

Our algorithm is very fast for color image segmentation, but similar to other k-means clustering algorithms, it has limitations in practical applications since the number of clusters must be set prior. In the future work, we will explore fast clustering algorithms that automatically estimate the number of clusters [48], [49].

REFERENCES

[1] B. Abu-Jamous, R. Fa, and A. K. Nandi, *Integrative Cluster Analysis in Bioinformatics*. Hoboken, NJ, USA: Wiley, 2015.

[2] S. Zeng, X. Wang, H. Cui, C. Zheng, and D. Feng, "A unified collaborative multi-kernel fuzzy clustering for multiview data," *IEEE Trans. Fuzzy Syst.*, vol. 26, no. 3, pp. 1671–1687, Jun. 2018.

[3] J. Ma, S. Li, H. Qin, and A. Hao, "Unsupervised multi-class co-segmentation via joint-cut over L_1-manifold hyper-graph of discriminative image regions," *IEEE Trans. Image Process.*, vol. 26, no. 3, pp. 1216–1230, Mar. 2017.

[4] M. Gong, H. Li, X. Zhang, Q. Zhao, and B. Wang, "Nonparametric statistical active contour based on inclusion degree of fuzzy sets," *IEEE Trans. Fuzzy Syst.*, vol. 24, no. 5, pp. 1176–1192, Oct. 2016.

[5] M. Bai and R. Urtasun, "Deep watershed transform for instance segmentation," in *Proc. IEEE Conf. Comput. Vis. Pattern Recognit.*, Honolulu, HI, USA, 2017, pp. 2858–2866.

[6] M. Pereyra and S. McLaughlin, "Fast unsupervised Bayesian image segmentation with adaptive spatial regularisation," *IEEE Trans. Image Process.*, vol. 26, no. 6, pp. 2577–2587, Jun. 2017.

[7] S. Yin, Y. Qian, and M. Gong, "Unsupervised hierarchical image segmentation through fuzzy entropy maximization," *Pattern Recognit.*, vol. 68, pp. 245–259, Aug. 2017.

[8] A. Krizhevsky, I. Sutskever, and G. E. Hinton, "Imagenet classification with deep convolutional neural networks," in *Proc. Adv. Neural Inf. Proc. Syst.*, New York, NY, USA, 2012, pp. 1097–1105.

[9] E. Shelhamer, J. Long, and T. Darrell, "Fully convolutional networks for semantic segmentation," *IEEE Trans. Pattern Anal. Mach. Intell.*, vol. 39, no. 4, pp. 640–651, Apr. 2017.

[10] N. R. Pal and J. C. Bezdek, "On cluster validity for the fuzzy c-means model," *IEEE Trans. Fuzzy Syst.*, vol. 3, no. 3, pp. 370–379, Aug. 1995.

[11] D. Comaniciu and P. Meer, "Mean shift: A robust approach toward feature space analysis," *IEEE Trans. Pattern Anal. Mach. Intell.*, vol. 24, no. 5, pp. 603–619, May 2002.

[12] A. Y. Ng, M. I. Jordan, and Y. Weiss, "On spectral clustering: Analysis and an algorithm," in *Proc. Adv. Neural Inf. Proc. Syst.*, Vancouver, BC, USA, 2001, pp. 849–856.

[13] Y. Zhang, X. Bai, R. Fan, and Z. Wang, "Deviation-sparse fuzzy c-means with neighbor information constraint," *IEEE Trans. Fuzzy Syst.*, 2018. doi: 10.1109/TFUZZ.2018.2883033.

[14] J. Fan and J. Wang, "A two-phase fuzzy clustering algorithm based on neurodynamic optimization with its application for PolSAR image segmentation," *IEEE Trans. Fuzzy Syst.*, vol. 26, no. 1, pp. 72–83, Feb. 2018.

[15] R. Shang, P. Tian, L. Jiao, R. Stolkin, B. Hou, and X. Zhang, "A spatial fuzzy clustering algorithm with kernel metric based on immune clone for SAR image segmentation," *IEEE J. Sel. Topics Appl. Earth Observ.*, vol. 9, no. 4, pp. 1640–1652, Apr. 2016.

[16] M. N. Ahmed, S. M. Yamany, N. Mohamed, A. A. Farag, and T. Moriarty, "A modified fuzzy c-means algorithm for bias field estimation and segmentation of MRI data," *IEEE Trans. Med. Imag.*, vol. 21, no. 3, pp. 193–199, Mar. 2002.

[17] S. Chen and D. Zhang, "Robust image segmentation using FCM with spatial constraints based on new kernel-induced distance measure," *IEEE Trans. Syst., Man, Cybern., B, Cybern.*, vol. 34, no. 4, pp. 1907–1916, Aug. 2004.

[18] W. Cai, S. Chen, and D. Zhang, "Fast and robust fuzzy c-means clustering algorithms incorporating local information for image segmentation," *Pattern Recognit.*, vol. 40, no. 3, pp. 825–838, Mar. 2007.

[19] S. Krinidis and V. Chatzis, "A robust fuzzy local information c-means clustering algorithm," *IEEE Trans. Image Process.*, vol. 19, no. 5, pp. 1328–1337, May 2010.

[20] Z. Zhao, L. Cheng, and G. Cheng, "Neighbourhood weighted fuzzy c-means clustering algorithm for image segmentation," *IET Image Process.*, vol. 8, no. 3, pp. 150–161, Mar. 2014.

[21] F. Guo, X. Wang, and J. Shen, "Adaptive fuzzy c-means algorithm based on local noise detecting for image segmentation," *IET Image Process.*, vol. 10, no. 4, pp. 272–279, Apr. 2016.

[22] K. H. Memon and D. H. Lee, "Generalised fuzzy c-means clustering algorithm with local information," *IET Image Process.*, vol. 11, no. 1, pp. 1–12, Jan. 2017.

[23] M. Gong, Y. Liang, J. Shi, W. Ma, and J. Ma, "Fuzzy c-means clustering with local information and kernel metric for image segmentation," *IEEE Trans. Image Process.*, vol. 22, no. 2, pp. 573–584, Feb. 2013.

[24] G. Liu, Y. Zhang, and A. Wang, "Incorporating adaptive local information into fuzzy clustering for image segmentation," *IEEE Trans. Image Process.*, vol. 24, no. 11, pp. 3990–4000, Nov. 2015.

[25] X. Bai, Z. Chen, Y. Zhang, Z. Liu, and Y. Lu, "Infrared ship target segmentation based on spatial information improved FCM," *IEEE Trans. Cybern.*, vol. 46, no. 12, pp. 3259–3271, Dec. 2016.

[26] H. Zhang, Q. Wang, W. Shi, and M. Hao, "A novel adaptive fuzzy local information c-means clustering algorithm for remotely sensed imagery classification," *IEEE Trans. Geosci. Remote Sens.*, vol. 55, no. 9, pp. 5057–5068, Sep. 2017.

[27] P. Ghamisi, J. A. Benediktsson, and M. O. Ulfarsson, "Spectral-spatial classification of hyperspectral images based on hidden Markov random fields," *IEEE Trans. Geosci. Remote Sens.*, vol. 52, no. 5, pp. 2565–2574, May 2014.

[28] Q. Zhao, X. Li, Y. Li, and X. Zhao, "A fuzzy clustering image segmentation algorithm based on hidden Markov random field models and voronoi tessellation," *Pattern Recognit. Lett.*, vol. 85, no. 1, pp. 49–55, Jan. 2017.

[29] G. Liu, Z. Zhao, and Y. Zhang, "Image fuzzy clustering based on the region-level Markov random field model," *IEEE Geosci. Remote Sens. Lett.*, vol. 12, no. 8, pp. 1770–1774, Aug. 2015.

[30] S. P. Chatzis and T. A. Varvarigou, "A fuzzy clustering approach toward hidden Markov random field models for enhanced spatially constrained image segmentation," *IEEE Trans. Fuzzy Syst.*, vol. 16, no. 5, pp. 1351–1361, Oct. 2008.

[31] H. Zhang, Q. M. J. Wu, Y. Zheng, T. M. Nguyen, and D. Wang, "Effective fuzzy clustering algorithm with Bayesian model and mean template for image segmentation," *IET Image Process.*, vol. 8, no. 10, pp. 571–581, Oct. 2014.

[32] T. Lei, X. Jia, Y. Zhang, L. He, H. Meng, and A. K. Nandi, "Significantly fast and robust fuzzy c-means clustering algorithm based on morphological reconstruction and membership filtering," *IEEE Trans. Fuzzy Syst.*, vol. 26, no. 5, pp. 3027–3041, Oct. 2018.

[33] T. Lei, Y. Zhang, Y. Wang, S. Liu, and Z. Guo, "A conditionally invariant mathematical morphological framework for color images," *Inf. Sci.*, vol. 387, pp. 34–52, May 2017.

[34] M. Liu, O. Tuzel, S. Ramalingam, and R. Chellappa, "Entropy rate superpixel segmentation," in *Proc. IEEE Conf. Comput. Vis. Pattern Recognit.*, Colorado Springs, CO, USA, 2011, pp. 2097–2104.

[35] S. Wang, H. Lu, F. Yang, and M. Yang, "Superpixel tracking," in *Proc. IEEE Int. Conf. Comput. Vis.*, Barcelona, Spain, 2011, pp. 1323–1330.

[36] S. Kim, C. D. Yoo, S. Nowozin, and P. Kohli, "Image segmentation using higher-order correlation clustering," *IEEE Trans. Pattern Anal. Mach. Intell.*, vol. 36, no. 9, pp. 1761–1774, Sep. 2014.

[37] J. Chen, Z. Li, and B. Huang, "Linear spectral clustering superpixel," *IEEE Trans. Image Process.*, vol. 26, no. 7, pp. 3317–3330, Jul. 2017.

[38] L. Szilágyi, Z. Benyó, S. Szilágyi, and H. Adam, "MR brain image segmentation using an enhanced fuzzy c-means algorithm," in *Proc. 25th Annu. Int. Conf. IEEE Eng. Med. Biol. Soc.*, Cancun, Mexico, 2003, pp. 724–726.

[39] D. Özdemir and L. Akarun, "A fuzzy algorithm for color quantization of images," *Pattern Recognit.*, vol. 35, no. 8, pp. 1785–1791, Aug. 2002.

[40] R. Achanta, A. Shaji, K. Smith, A. Lucchi, P. Fua, and S. Susstrunk, "SLIC superpixels compared to state-of-the-art superpixel methods," *IEEE Trans. Pattern Anal. Mach. Intell.*, vol. 34, no. 11, pp. 2274–2282, Nov. 2012.

[41] Z. Hu, Q. Zou, and Q. Li, "Watershed superpixel," in *Proc. IEEE Int. Conf. Image Process.*, Quebec City, QC, USA, 2015, pp. 349–353.

[42] T. H. Kim, K. M. Lee, and S. U. Lee, "Learning full pairwise affinities for spectral segmentation," *IEEE Trans. Pattern Anal. Mach. Intell.*, vol. 35, no. 7, pp. 1690–1703, Jul. 2013.

[43] B. Wang and Z. Tu, "Affinity learning via self-diffusion for image segmentation and clustering," in *Proc. IEEE Conf. Comput. Vis. Pattern Recognit.*, Providence, RI, USA, 2012, pp. 2312–2319.

[44] L. Vincent, "Morphological Grayscale reconstruction in image analysis: applications and efficient algorithms," *IEEE Trans. Image Process.*, vol. 2, no. 2, pp. 176–201, Apr. 1993.

[45] P. Arbelaez, M. Maire, C. Fowlkes, and J. Malik, "Contour detection and hierarchical image segmentation," *IEEE Trans. Pattern Anal. Mach. Intell.*, vol. 33, no. 5, pp. 898–916, May 2011.

[46] J. Shotton, J. Winn, C. Rother, and A. Criminisi, "Textonboost: Joint appearance, shape and context modeling for multi-class object recognition and segmentation," in *Proc. Eur. Conf. Comput. Vis.*, Graz, Austria, 2006, pp. 1–15.

[47] X. Wang, Y. Tang, S. Masnou, and L. Chen, "A global/local affinity graph for image segmentation," *IEEE Trans. Image Process.*, vol. 24, no. 4, pp. 1399–1411, Apr. 2015.

[48] A. Rodriguez and A. Laio, "Clustering by fast search and find of density peaks," *Science*, vol. 344, no. 6191, pp. 1492–1496, Jun. 2014.

[49] J. Hou and W. X. Liu, "A parameter independent clustering framework,"*IEEE Trans. Ind. Informat.*, vol. 13, no. 4, pp. 1825–1832, Aug. 2017.

Tao Lei (M'17) received the Ph.D. degree in information and communication engineering from Northwestern Polytechnical University, Xi'an, China, in 2011.

From 2012 to 2014, he was a Postdoctoral Research Fellow with the School of Electronics and Information, Northwestern Polytechnical University, Xi'an, China. From 2015 to 2016, he was a Visiting Scholar with the Quantum Computation and Intelligent Systems Group, University of Technology Sydney, Sydney, Australia. He is currently a Professor with the School of Electrical and Information Engineering, Shaanxi University of Science and Technology, Xi'an, China. His current research interests include image processing, pattern recognition, and machine learning.

Xiaohong Jia received the M.S. degree in signal and information processing from Lanzhou Jiaotong University, Lanzhou, China, in 2017. He is currently working toward the Ph.D. degree with the School of Electronical and Information Engineering, Shaanxi University of Science and Technology, Xi'an, China.

His current research interests include image processing and pattern recognition.

Yanning Zhang (M'08–SM'12) received the B.S. degree in electronic engineering from Dalian University of Technology, Dalian, China, in 1988, and the Ph.D. degree in signal and information processing from Northwestern Polytechnical University, Xi'an, China, in 1996.

She is currently a Professor with the School of Computer Science, Northwestern Polytechnical University. Her current research interests include computer vision and pattern recognition, image and video processing, and intelligent information processing. She was the Organization Chair of the Asian Conference on Computer Vision 2009. She served as the Program Committee Chair of several international conferences.

Shigang Liu received the B.S. and M.S. degrees from Harbin Engineering University, Harbin, China, in 1997 and 2001, respectively. He received the Ph.D. degrees from Xidian University of China, Xi'an, China, in 2005.

From 2009 to 2010, he was a visiting scholar with the Department of Computing, Hong Kong Polytechnic University. From 2015 to 2016, he was a visiting scholar with the Quantum Computation and Intelligent System Group, University of Technology Sydney, Sydney, Australia. He is currently a Professor with the School of Computer Science, Shaanxi Normal University, Xi'an, China. His research interests include pattern recognition and image processing.

Hongying Meng (M'10–SM'17) received the Ph.D. degree in communication and electronic systems from Xi'an Jiaotong University, Xi'an, China, in 1998.

He is currently a Senior Lecturer with the Department of Electronic and Computer Engineering, Brunel University, London, U.K. He is also a member of Institute of Environment, Health and Societies, Human Centred Design Institute, and Wireless Networks and Communications Research Center, Brunel. His current research interests include digital signal processing, affective computing, machine learning, human–computer interaction, computer vision, and embedded systems with over 90 publications in these areas.

Dr. Meng's audio-based and video-based emotion recognition systems have won the International Audio/Visual Emotion Challenges AVEC2011 and AVEC2013 prizes, respectively. He is a Fellow of The Higher Education Academy and a member of Engineering Professors Council in UK.

Asoke K. Nandi (F'11) received the Ph.D. degree in physics from the University of Cambridge (Trinity College), Cambridge, U.K.

He held academic positions in several universities, including University of Oxford, Oxford, U.K., Imperial College London, London, U.K., University of Strathclyde, Glasgow, U.K, and University of Liverpool, Liverpool, U.K., as well as Finland Distinguished Professorship in Jyvaskyla, Finland. In 2013, he moved to Brunel University, London, U.K., to become the Chair and Head of Electronic and Computer Engineering. He is a Distinguished Visiting Professor with Tongji University, Shanghai, China and an Adjunct Professor with the University of Calgary, Calgary, AB, Canada. His current research interests include the areas of signal processing and machine learning, with applications to communications, gene expression data, functional magnetic resonance data, and biomedical data. He has made many fundamental theoretical and algorithmic contributions to many aspects of signal processing and machine learning. He has much expertise in "Big Data," dealing with heterogeneous data, and extracting information from multiple data sets obtained in different laboratories and different times. He has authored more than 570 technical publications, including 230 journal papers as well as four books, entitled *Automatic Modulation Classification: Principles, Algorithms and Applications* (Wiley, 2015), *Integrative Cluster Analysis in Bioinformatics* (Wiley, 2015), *Blind Estimation Using Higher-Order Statistics* (Springer, 1999), and *Automatic Modulation Recognition of Communications Signals* (Springer, 1996).

Prof. Nandi is a Fellow of the Royal Academy of Engineering (U.K.) and also a Fellow of seven other institutions, including the IET. He received the Institute of Electrical and Electronics Engineers (USA) Heinrich Hertz Award in 2012, the Glory of Bengal Award for his outstanding achievements in scientific research in 2010, the Water Arbitration Prize of the Institution of Mechanical Engineers (U.K.) in 1999, and the Mountbatten Premium, Division Award of the Electronics and Communications Division, of the Institution of Electrical Engineers (U.K.) in 1998. In 1983, he co-discovered the three fundamental particles known as W^+, W^-, and Z^0, providing the evidence for the unification of the electromagnetic and weak forces, for which the Nobel Committee for Physics in 1984 awarded the prize to his two team leaders for their decisive contributions. Recently, he published in *Blood*, *International Journal of Neural Systems*, *BMC Bioinformatics*, IEEE TRANSACTIONS ON WIRELESS COMMUNICATIONS, *NeuroImage*, *PLOS ONE*, *Royal Society Interface*, *Mechanical systems and Signal Processing*, and *Molecular Cancer*. The h-index of his publications is 70 (Google Scholar) and ERDOS number is 2. He is an IEEE EMBS Distinguished Lecturer (2018–2019).